Journal of Materials Chemistry C

Solution-Processable All-Small Molecular Bulk Heterojunction Films for Stable Organic Photodetectors: Near UV and Visible Light Sensing

Journal:	*Journal of Materials Chemistry C*
Manuscript ID:	TC-ART-09-2014-002194.R1
Article Type:	Paper
Date Submitted by the Author:	30-Oct-2014

Complete List of Authors:	Lee, Hyena; Kyungpook National University, Department of Chemical Engineering Nam, Sungho; Kyungpook National University, Department of Chemical Engineering Kwon, Hyunju; Kyungpook National University, Department of Chemical Engineering Lee, Sooyong; Kyungpook National University, Department of Chemical Engineering Kim, Jungnam; Kyungpook National University, Department of Chemical Engineering Lee, Woongki; Kyungpook National University, Department of Chemical Engineering Lee, Chulyeon; Kyungpook National University, Department of Chemical Engineering Jeong, Jaehoon; Kyungpook National University, Department of Chemical Engineering Kim, Hwajeong; Kyungpook National University, Department of Chemical Engineering Shin, Taejoo; Pohang Accelerator Laboratory, Kim, YoungKyoo; Kyungpook National University, Department of Chemical Engineering

Journal of Materials Chemistry C RSCPublishing

ARTICLE

Solution-Processable All-Small Molecular Bulk Heterojunction Films for Stable Organic Photodetectors: Near UV and Visible Light Sensing

Cite this: DOI: 10.1039/x0xx00000x

Received 00th January 2014,
Accepted 00th January 2014

DOI: 10.1039/x0xx00000x

www.rsc.org/

Hyena Lee,[a] Sungho Nam,[a] Hyunju Kwon,[a] Sooyong Lee,[a] Jungnam Kim,[a] Woongki Lee,[a] Chulyeon Lee,[a] Jaehoon Jeong,[a] Hwajeong Kim,[b] Tae Joo Shin[c] and Youngkyoo Kim*[a]

We report stable organic photodetectors with all-small molecular bulk heterojunction (BHJ) sensing layers prepared using solutions of electron-donating and electron-accepting small molecules. As an electron-donating molecule 2,5-bis(2-ethylhexyl)-3,6-bis(4'-methyl-[2,2'-bithiophen]-5-yl)pyrrolo[3,4-c]pyrrole-1,4(2H,5H)-dione (EHTPPD-MT) was synthesized via Stille coupling reaction, while [6,6]-phenyl-C_{61}-butyric acid methyl ester ($PC_{61}BM$) was used as an electron-accepting component. The devices with the EHTPPD-MT:$PC_{61}BM$ BHJ layer could detect photons at a wavelength of 400~800 nm and exhibited a stable photoresponse under on/off modulation of near UV (405 nm) and visible (532 nm and 650 nm) lights even at bias voltage condition. The corrected responsivity reached ~175 mA/W for the near UV detection at -1 V. An extremely durable photoresponse was measured for the present devices (including flexible devices) under illumination of a high intensity green light (133.4 mW/cm^2 at 532 nm) which is much stronger than the standard sun light (100 mW/cm^2, white). The excellent stability has been attributed to the tiny EHTPPD-MT crystals, which are formed in the EHTPPD-MT:$PC_{61}BM$ layers during the coating processes.

Introduction

Organic photodetectors (OPDs) have recently attracted keen attention because of their potential for lightweight and flexible photodetector modules in the coming flexible electronics era since successful commercialization of organic light-emitting devices (OLEDs) for smart phones and large-size high definition TVs.[1-5] In principle, OPDs can detect various ranges of light by employing suitable organic semiconducting materials as a sensing medium (active layer), which can be achieved by designing their chemical structures in the synthesis process.[6-8] Compared to conventional photodetectors with inorganic semiconducting materials, OPDs have a strong benefit in the facile control of detection band (wavelength range) by simple mixing of more than two organic semiconducting materials in solutions.[3,9,10]

To date, two types of OPDs, a diode type and a transistor type, have been studied using either small molecules or polymers.[4,5,11-14] Organic photodiodes (OPDIs) have a merit of large detection area because organic semiconducting layers can be placed between two parallel (top and bottom) electrodes, whereas organic phototransistors (OPTRs) have a limited detection area owing to typically narrow channel length (< 150 μm) (note that additional high accuracy processes are required for further extension of detection area leading to organic phototransistors with an interdigitated structure).[15,16] In addition, the simple device structure of OPDIs delivers further advantages of low-cost and easy fabrication processes.

Both small molecules and polymers have been employed as an active layer for OPDIs.[4,5,17-22] Most of early works have used single materials as an active layer for OPDIs so that the device efficiency was quite low because of low charge separation yields owing to the absence of internal driving force for charge separation.[23,24] To overcome this problem, a bulk heterojunction (BHJ) layer has been introduced into OPDIs as used for organic solar cells.[25-28] The representative BHJ materials used for OPDIs so far are: (1) poly[N-9′-heptadecanyl-2,7-carbazole-alt-5,5-(4′,7′-di-2-thienyl-2′,1′,3′-benzothiadiazole)] (PCDTBT) and [6,6]-phenyl-C_{61}-butyric acid methyl ester ($PC_{61}BM$), (2) poly(9,9'-dioctylfluorene-co-benzothiadiazole) (F8BT) and N,N'-bis(alkyl)-3,4,9,10-perylenetetracarboxylicdiimide (PDI), (3) poly(3-hexylthiophene-2,5-diyl) (P3HT) and $PC_{61}BM$, (4) 7,7'-(4,4-bis(2-ethylhexyl)-4H-silolo[3,2-b:4,5-b']dithiophene-2,6-diyl)bis(6-fluoro-4-(5′-hexyl-[2,2'-bithiophen]-5-yl)benzo[c][1,2,5]thiadiazole) (p-DTS(FBTTh$_2$)$_2$) and [6,6]-phenyl-C_{71}-butyric acid methyl ester ($PC_{71}BM$), (5) symmetric squarines and $PC_{61}BM$, (6) 5,15-bis-(7-(4-hexylthiophen-2-yl)-2,1,3-benzothiadiazole-4-yl-ethynyl)-10,20-bis(3,5-di(dodecyloxy)-phenyl)-porphyrin zinc (DHTBTEZP) and $PC_{61}BM$, (7) 2,5-bis(2,5-(bis(2-thienyl)-N-*alkyl* pyrrole)thieno[3,5-b][1,2,5]thiadiazole and $PC_{61}BM$, (8) quinquethiophene-cored conjugated dendrimers and $PC_{61}BM$.[29-

[a]Organic Nanoelectronics Laboratory, Department of Chemical Engineering, Kyungpook National University, Daegu 702-701, Republic of Korea
E-mail: ykimm@knu.ac.kr
[b]Priority Research Center, Research Institute of Advanced Energy Technology, Kyungpook National University, Daegu 702-701, Republic of Korea
[c]Pohang Accelerator Laboratory,Pohang 790-784, Republic of Korea

[36] However, no study has been carried out for the stability of OPDIs under illumination of high intensity lights.

In this work, we attempted to fabricate OPDIs with all-small molecular BHJ layers that can be prepared by wet-coating process using solutions of electron-donating (p-type) and electron-accepting (n-type) small molecules. As the p-type small molecule, 2,5-bis(2-ethylhexyl)-3,6-bis(4'-methyl-[2,2'-bithiophen]-5-yl)pyrrolo[3,4-c]pyrrole-1,4(2H,5H)-dione (EHTPPD-MT), which has a shorter alkyl chain (methyl group) compared to the recently reported 2,5-bis(2-ethylhexyl)-3,6-bis(4'-hexyl-[2,2']-bithiophen-5-yl)pyrrolo[3,4-c]pyrrole-1,4(2H,5H)-dione,[37] was synthesized via Stille coupling reaction in this work. As the n-type material, [6,6]-phenyl-C_{61}-butyric acid methyl ester ($PC_{61}BM$) was used because of its outstanding electron-accepting and film-forming characteristics.[38-41] Two compositions (EHTPPD-MT:$PC_{61}BM$ = 1:2 and 1:3 by weight) were employed for the fabrication of OPDIs, while near UV (405 nm) and two visible (532 nm and 650 nm) lights were used to test the performance of the present OPDIs. A high intensity green light (133.4 mW/cm^2 at 532 nm), which is a monochromatic but much stronger than the standard one sun light (100 mW/cm^2, white), was employed to examine the stability of devices under illumination of high intensity light. The nanostructure of the EHTPPD-MT:$PC_{61}BM$ layers was investigated with high resolution scanning electron microscopy (SEM), transmission electron microscopy (TEM) and synchrotron grazing incidence angle X-ray diffraction (GIXD) measurements.

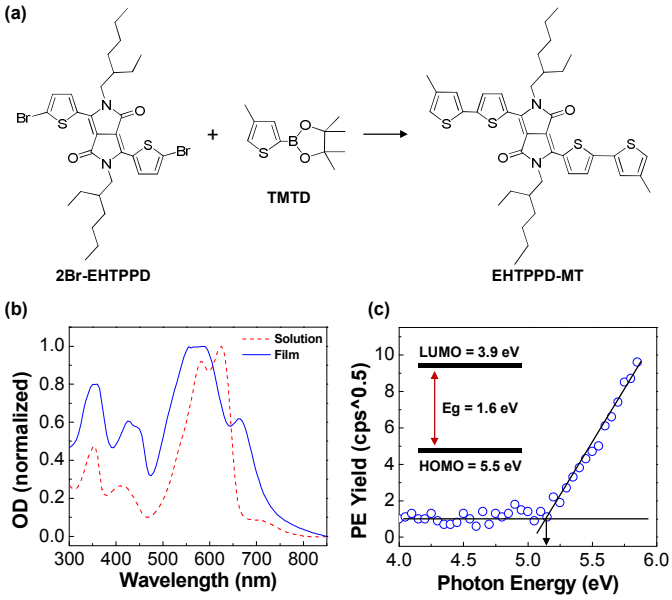

Fig. 1 (a) Scheme for the synthesis of 2,5-bis(2-ethylhexyl)-3,6-bis(4'-methyl-[2,2'-bithiophen]-5-yl)pyrrolo[3,4-c]pyrrole-1,4(2H,5H)-dione (EHTPPD-MT) from 3,6-bis(5-bromo-2-thienyl)-2,5-dihexadecyl-2,5-dihydropyrrolo[3,4-c]pyrrole-1,4-dione (2Br-EHTPPD) and 3-methyl-thiophene-2-boronic acid pinacol ester (TMTD). The detailed synthesis procedures are explained in the experimental section. (b) Optical density (OD) of the EHTPPD-MT solution and film as a function of wavelength. (c) Photoelectron (PE) yield spectrum of the EHTPPD-MT coated on quartz substrate: Inset shows the flat energy band diagram for EHTPPD-MT (note that minus signs in the energy values were omitted).

Results and Discussion

The EHTPPD-MT material (dark pale blue color) was synthesized via Stille coupling reaction of 3,6-bis(5-bromothiophen-2-yl)-2,5-bis(2-ethylhexyl)pyrrolo[3,4-c]pyrrole-1,4(2H,5H)-dione(2Br-EHTPPD) and 3-methyl-thiophene-2-boronic acid pinacol ester (TMTD) (see the scheme in Fig. 1a). The detailed synthesis procedures are described in the experimental section. As shown in Fig. 1b, the EHTPPD-MT material has much wider absorption in film than in solution due to the relatively high optical density at the wavelengths below 450 nm and above 650 nm (see Fig. S1 for solvent). In particular, it is worthy to note that the absorption edge (tail) of the EHTPPD-MT film reached ca. 800 nm. Based on the onset point of the absorption tail in solution (see Fig. S2), the band gap energy of the EHTPPD-MT molecule was calculated ~1.6 eV (note that the optical band gap energy of the EHTPPD-MT film is expected to be ~1.5 eV because of its longer tail). The highest occupied molecular orbital (HOMO) energy of EHTPPD-MT (~5.5 eV) was obtained from the photoelectron yield spectrum of the EHTPPD-MT film after calibration (Fig. 1c).[42,43] Thus the lowest unoccupied molecular orbital (LUMO) energy (3.9 eV) of EHTPPD-MT could be obtained by subtracting the band gap energy (1.6 eV) from the HOMO energy (5.5 eV) (see inset in Fig. 1c).

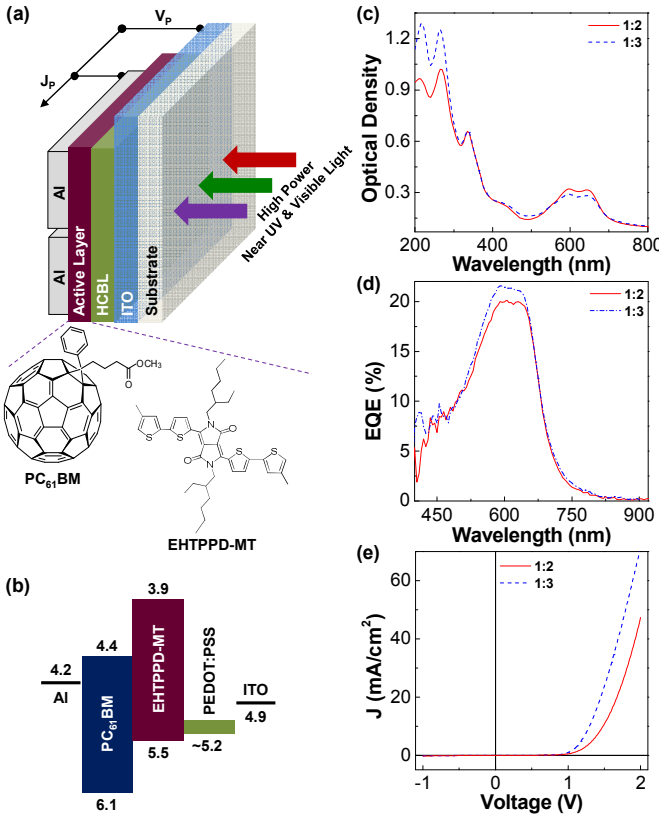

Fig. 2 (a) Device structure and materials used for the fabrication of organic photodiodes (OPDIs) in this work. (b) Flat energy band diagram for the present device (note that minus "-" sign and "eV" unit were omitted in order to avoid crowding the diagram). (c) Optical density (OD) as a function of wavelength for the EHTPPD-MT:$PC_{61}BM$ films on quartz substrates. (d) External quantum efficiency (EQE) spectra for the OPDIs with the solution-processed EHTPPD-MT:$PC_{61}BM$ layers at 0 V. (e) Dark current density–voltage (J-V) characteristics for the OPDIs with the solution-processed EHTPPD-MT:$PC_{61}BM$ layers.

Hence EHTPPD-MT was used as a p-type (electron-donating) component in the solution-processed EHTPPD-MT:$PC_{61}BM$ BHJ layers for OPDIs, because the LUMO energy level of EHTPPD-MT is lower (negatively) than that of $PC_{61}BM$ (see Fig. 2ab). In brief, as seen from the structure of OPDIs, the incident light passes through the glass substrate/ITO/PEDOT:PSS layers and finally arrives at the BHJ (EHTPPD-MT:$PC_{61}BM$) layer. Once excitons are generated by light absorption and charge separation processes occur in the EHTPPD-MT:$PC_{61}BM$ layer, the individual charges (holes and electrons) transport toward corresponding electrodes by the driving forces (built-in electric field and photovoltage) inside the OPDIs. Considering the optical absorption spectra of the EHTPPD-MT:$PC_{61}BM$ layers (1:2 and 1:3 by weight ratio) in Fig. 2c (see Fig. S3 for the absorption spectrum of the pristine $PC_{61}BM$ film), the present active layers can detect photons from 200 nm to 800 nm. However, the actual absorption range is limited from ca. 350 nm to 800 nm because of the absorption by the glass substrate below ca. 350 nm. As shown in the external quantum efficiency (EQE) spectra measured at 0 V (Fig. 2d), an EQE tail covers up 800 nm even though the EQE value over 750 nm is quite low. Here we note that the EQE maximum was slightly higher for the 1:3 (EHTPPD-MT:$PC_{61}BM$) composition than the 1:2 composition, which is a contrast to the optical absorption trend in Fig. 2c. The reason can be attributed to the better charge transport for the 1:3 composition than the 1:2 composition as seen from the current density – voltage (J-V) characteristics in the dark (see Fig. 2e).

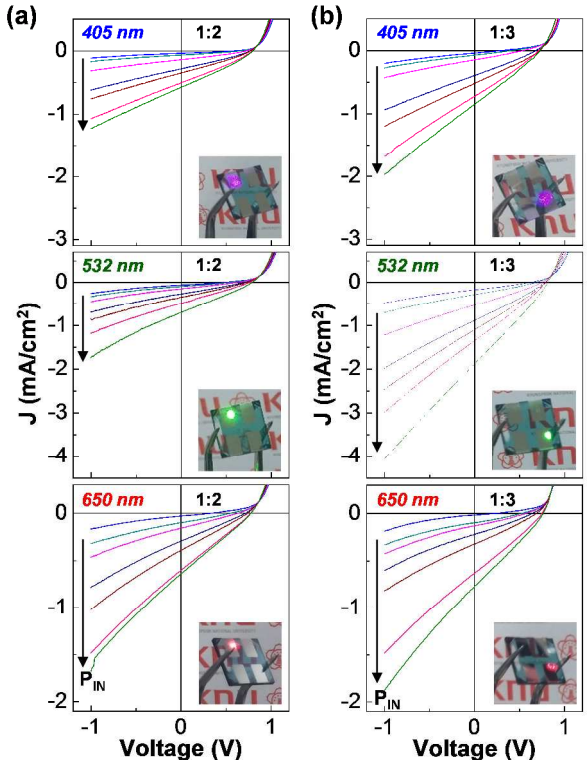

Fig. 3 Light J-V characteristics of devices under illumination of near UV (405 nm), green (532 nm) and red (650 nm) lights: (a) OPDIs with the EHTPPD-MT:$PC_{61}BM$ (1:2) layers. (b) OPDIs with the EHTPPD-MT:$PC_{61}BM$ (1:3) layers. P_{IN} (mW/cm^2 from top to bottom in each graph): (405 nm) 1.0, 2.0, 4.1, 8.2, 10.2, 14.3 and 16.4; (532 nm) 1.7, 3.4, 6.9, 10.3, 13.7, 17.2 and 24.0; (650 nm) 0.4, 1.9, 3.7, 11.1, 14.8, 26.0 and 30.0. Inset photographs show OPDIs under illumination of corresponding incident lights for demonstration only (note that actual measurements were carried out by mounting the OPDIs inside an argon-filled sample holder and the incident light beam was perfectly aligned into the active area of devices).

Based on the optical absorption and EQE spectra discussed in Fig. 2, near UV (405 nm) and two visible lights (green - 532 nm; red - 650 nm) were selected as a light source for the examination of the present OPDIs. Here it is noteworthy that the near UV light (405 nm) detection is of high interest because of recently commercialized high-power UV light-emitting diode (UV LED) systems which feature compact and long lifetime so that they are expected to replace conventional UV lamps for photolithography and curing processes etc.[44,45] As shown in the J-V curves (Fig. 3), the current density was greatly increased (negatively) as the incident light intenisty (P_{IN}) increased irrespective of wavelengths and compositions. This result indicates that the present OPDIs do properly work under illumination of common visible (green and red) lights as well as near UV light (405 nm). In particular, we find that the photocurrent increase was more pronounced for the 1:3 composition (Fig. 3b) than the 1:2 composition (Fig. 3a), which is basically in accordance with the EQE spectra (see Fig. 2d). However, the current density became greater (negatively) at higher voltages than lower voltages (negative), leading to the noticeable steep slopes in the J-V curves. This result indicates that the charge transport is quite limited inside the BHJ layers owing to high charge blocking resistances between EHTPPD-MT and $PC_{61}BM$ molecules, which reflects that the present BHJ layers have further potential for optimization leading to better efficiency.

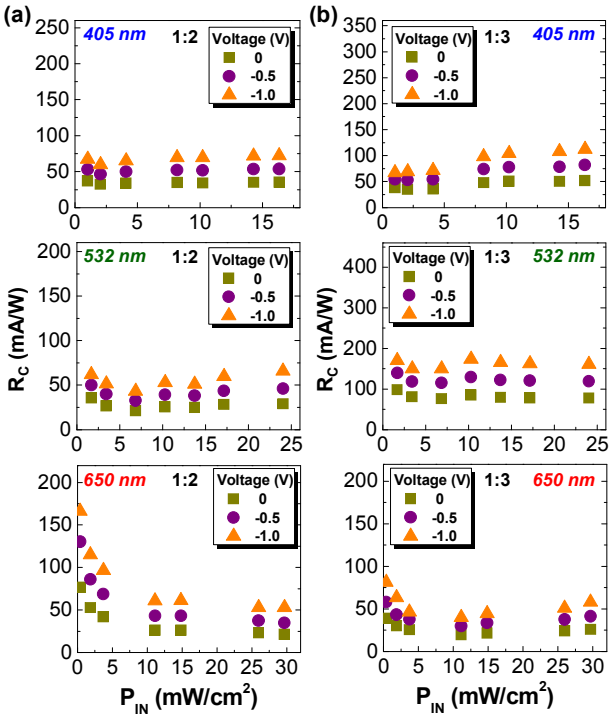

Fig. 4 Corrected responsivity (R_C) as a function of the incident light intensity (P_{IN}) under illumination of near UV (405 nm), green (532 nm) and red (650 nm) lights: (a) OPDIs with the EHTPPD-MT:$PC_{61}BM$ (1:2) layers. (b) OPDIs with the EHTPPD-MT:$PC_{61}BM$ (1:3) layers.

From the J-V curves in Fig. 3, the corrected responsivity (R_C = $(J_L-J_D)/P_{IN}$) was extracted after subtracting the dark current density (J_D) from the light current density (J_L) in order to understand the pure contribution of incident light without the intrinsic dark current in the devices. As shown in Fig. 4, the R_C value was increased as the applied voltage increased for all wavelengths. Interestingly, the R_C value was not seriously decreased even at higher intensity of near

UV light (405 nm) for both compositions. This trend was similar for the case of visible lights (532 nm and 650 nm). Considering the stable responsivity trend under illumination of such high intensity (16 ~ 30 mW/cm^2) of monochromatic (near UV and visible) lights, the present OPDIs are suitable for high power light detection even though the R_C value is relatively low. The maximum R_C value at -1 V was 112 mA/W (16.4 mW/cm^2 at 405 nm), 174 mA/W (10.3 mW/cm^2 at 532 nm), and 166 mA/W (0.4 mW/cm^2 at 650 nm).

Next, a brief operation performance was studied by measuring the photocurrent signals of the present OPDIs upon on/off modulation of the incident light (P_{IN} = 16.4 mW/cm^2 at 405 nm, 24.0 mW/cm^2 at 532 nm, 30.0 mW/cm^2 at 650 nm). As shown in Fig. 5, a stable photocurrent signal was measured for all wavelengths tested in this work. In addition, the photocurrent signal was still stable even at high applied voltages (up to -1 V) for both compositions, implying that the present OPDIs are suitable for bias-amplified detector applications. In particular, we need to pay keen attention to the result that the photocurrent signal was stable even under illumination of near UV light (405 nm) (see top panels in Fig. 5ab). This result supports that the present OPDIs can be applied as a low-cost integrated system-on detector for next generation near UV LED systems because of their solution process advantages leading to various detector shapes.

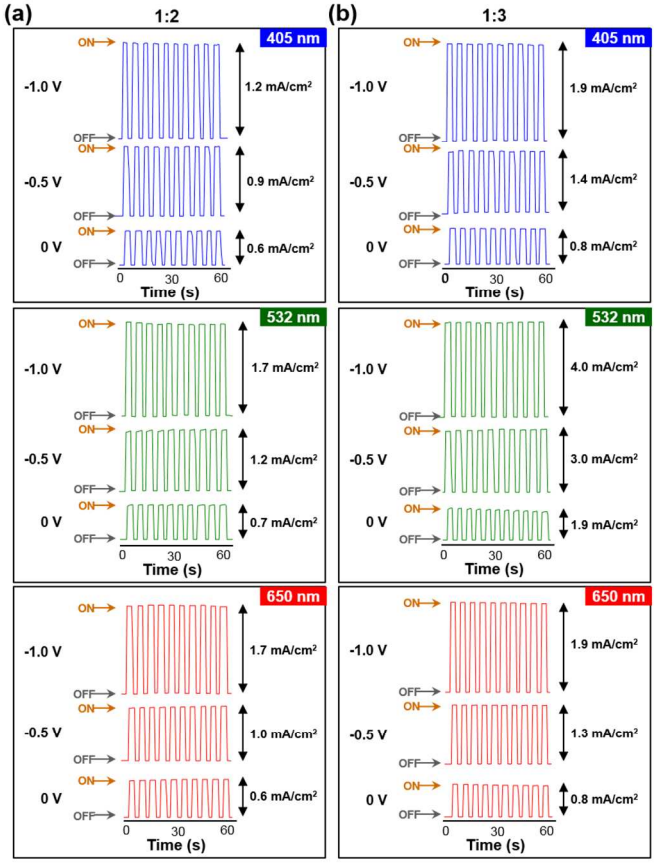

Fig. 5 Photoresponse characteristics of devices under on/off modulation of incident near UV (405 nm, P_{IN} = 16.4 mW/cm^2), green (532 nm, P_{IN} = 24 mW/cm^2) and red (650 nm, P_{IN} = 30 mW/cm^2) lights: (a) OPDIs with the EHTPPD-MT:PC_{61}BM (1:2) layers. (b) OPDIs with the EHTPPD-MT:PC_{61}BM (1:3) layers. The applied voltage is given on the left part of each pattern, while the photocurrent scale is given on the right part with arrows. The light modulation was carried out with a manual mode so that the pattern width (time scale) is slightly different each other.

To further examine the stability of the present OPDIs under illumination of much higher intensity light, one of the highest power green LED (133.4 mW/cm^2) was used to test the present OPDIs fabricated using the glass and flexible PET film subsrates. As shown in Fig. 6a, the present OPDIs exhibited clear J-V curves under the strong green light illumination for both compositions though the 1:3 composition was better than the 1:2 composition in terms of photocurrent generation, which is in agreement with the previou results. In particular, a stable photocurrent signal (ca. 100 signals) was measured from the present OPDIs upon on/off modulation of such strong visible light, which supports the high durability of the present OPDIs (see Fig. S4 for the quick on/off modulation case).

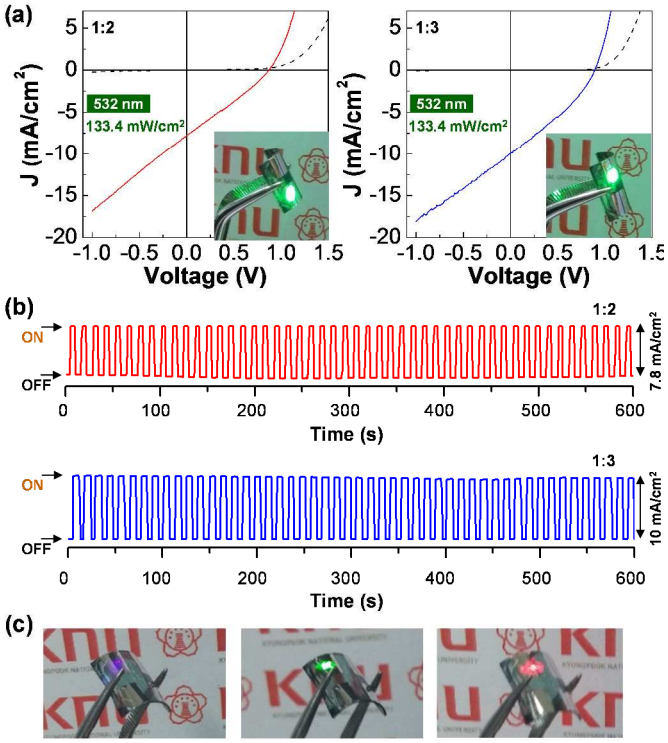

Fig. 6 Light J-V characteristics of devices under illumination of the high intensity green light (532 nm, P_{IN} = 133.4 mW/cm^2): (a) OPDIs with the EHTPPD-MT:PC_{61}BM (1:2 on the left and 1:3 on the right) layers. (b) Photoresponse characteristics of OPDIs under on/off modulation of the incident light at 0 V (note that the photoresponse patterns seem to be slow in the rise/decay shape owing to the slow on/off manual modulation but they were actually fast under fast on/off modulation as shown in Fig. S4). (c) Examples of flexible OPDIs with the EHTPPD-MT:PC_{61}BM layers by employing the PET film substrates under illumination of incident near UV (405 nm), green (532 nm) and red (650 nm) lights.

To understand the origin of such high device stability, we tried to investigate the nanostructure of the EHTPPD-MT:PC_{61}BM layer. As shown in Fig. 7a (left), a random crystalline morphology was measured from the pristine EHTPPD-MT film casted from its solution. Further maganification revealed that each crystal in the random crystalline structure is a nanorod with a diameter of less than 100 nm and various lengths. Interestingly, however, such big nanorods disappeared in the EHTPPD-MT:PC_{61}BM layer (see Fig. 7b), which can be attributed to the disturbed crystallization of EHTPPD-MT by the presence of PC_{61}BM owing to the well mixing between EHTPPD-MT and PC_{61}BM in the solution state. In other words, the EHTPPD-MT molecules in the BHJ layer might be

relatively easy to form its own nano-domains (leading to a mixed nanomorphology) instead of making such big nanorods in its pristine film (see the dark area in the TEM images in Fig. 7b). We note that the optical microscope (OM) examination could not find any particular micromorphology from the BHJ layer (see the OM image in the inset of Fig. 7b).

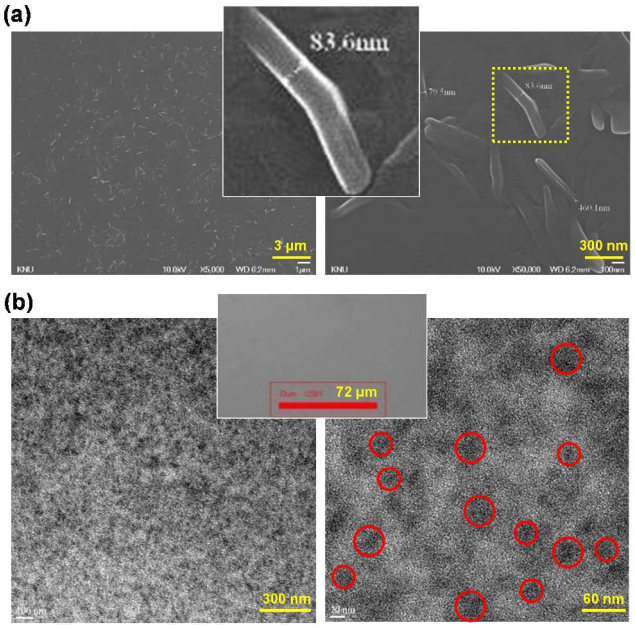

Fig. 7 (a) SEM images for the EHTPPD-MT material coated on glass substrate: (left) low magnification, (right) high magnification, and (middle) the enlarged image from the selected part marked with the dotted rectangle on the right image. (b) TEM images of the nanomorphology of the EHTPPD-MT:$PC_{61}BM$ (1:2) film: (left) low magnification, (right) high magnification, and (middle) optical microscope image for the present BHJ layer coated on the PEDOT:PSS layer on the ITO-glass substrate.

To further investigate the crystalline nanostructure in the EHTPPD-MT:$PC_{61}BM$ layer, the synchrotron radiation GIXD measurements were performed for the pristitine films and the BHJ films. As shown in the 2D GIXD images (Fig. 8), the pristine EHTPPD-MT film exhibited a particular diffraction pattern that corresponds to a well-ordered crystal structure as analyzed in Fig. S5. In contrast, the $PC_{61}BM$ film (as-coated but no thermal annealing) did not show any particular diffraction spots.[46] Interestingly, the diffraction spots of the EHTPPD-MT part became weakened in their intensity for the EHTPPD-MT:$PC_{61}BM$ (1:2) layer and some higher order diffraction spots did even disappear for the EHTPPD-MT:$PC_{61}BM$ (1:3) layer. This result is in good agreement with the TEM images in Fig. 7, which confirms again that the the EHTPPD-MT crystals might be prohibited by the presence of $PC_{61}BM$ molecules because of good compatability between EHTPPD-MT and $PC_{61}BM$. In addition to the weakened diffraction spots for the BHJ layers, we find from the 1D GIXD profiles that the major diffraction peak (100) of the EHTPPD-MT crystals was shifted toward lower angles for the BHJ films. This result indicates that the presence of $PC_{61}BM$ molecules did significantly affect the formation of the EHTPPD-MT crystals in the BHJ layers. Anyhow, these GIXD results deliver an important information that the present BHJ layers contain the EHTPPD-MT crystals even though their size and amount were different from the pristine EHTPPD-MT case. Hence the presence of the EHTPPD-MT crystals is considered to significantly contribute to the high stability of the present devices under illumination of high intensity lights.

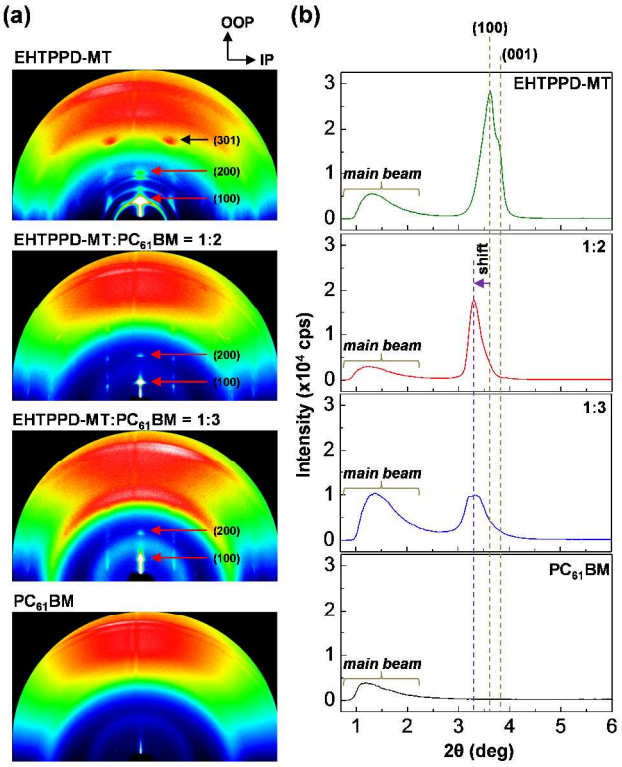

Fig. 8 (a) 2D GIXD images for films coated on the ITO-glass substrate. (b) 1D GIXD profiles in the out-of-plane (OOP) direction which were taken from the 2D GIXD images in (a). Note that the (100) diffraction peak of the EHTPPD-MT:$PC_{61}BM$ layers was shifted to a lower angle from that of the pristine EHTPPD-MT. No particular diffraction peak was measured for the $PC_{61}BM$ film because no thermal annealing was applied. The detailed diffraction peak assignment for the pristine EHTPPD-MT film is given in Fig. S5.

Conclusions

All-small molecular organic photodetectors were fabricated by solution processes using solutions of newly synthesized electron-donating EHTPPD-MT and conventional electron-accepting $PC_{61}BM$ molecules. The EHTPPD-MT film showed a broad optical absorption range from 300 nm to 800 nm, while its LUMO energy was 3.9 eV. The OPDIs with the EHTPPD-MT:$PC_{61}BM$ BHJ layers exhibited excellent rectification behavior in the dark, while they could detect photons in the near UV (405 nm) and whole visible ranges. Although the EQE of the present OPDIs was ca. 20% at 0 V, the photocurrent became greatly amplified under biased conditions (>0 V). The present OPDIs did sensitively work under illumination of near UV (405 nm) and two visible lights (532 nm and 650 nm) with various light intensities. The corrected responsivity after removing dark current contribution in the bias range of 0 V ~ -1 V reached 70~120 mA/W at 405 nm, 75~180 mA/W at 532 nm, and 80~170 mA/W at 650 nm. In particular, the present OPDIs exhibited stable responses under modulation of repeated incident lights for the three representative wavelengths (405 nm, 532 nm and 650 nm). Strikingly, the present OPDIs showed excellent durability under illumination of highly intense visible light (133.4 mW/cm^2 at 532 nm) that is too strong to see with naked eyes (much brighter than normal sun light). Such good performance and high stability in the

present OPDIs has been attributed to the formation of the EHTPPD-MT nanocrystal domains in the BHJ layers even though the crystal size and lattice of EHTPPD-MT were changed from its pristine form as disclosed from the TEM and GIXD measurements.

Experimental Section

***Synthesis and Solutions*:** 3,6-bis(5-bromo-2-thienyl)-2,5-dihexadecyl-2,5-dihydropyrrolo[3,4-c]pyrrole-1,4-dione (2Br-EHTPPD), 3-methyl-thiophene-2-boronic acid pinacol ester (TMTD) and potassium carbonate (K_2CO_3) were purchased from Sigma-Aldrich (USA). To synthesize 2,5-bis(2-ethylhexyl)-3,6-bis(4'-methyl-[2,2'-bithiophen]-5-yl)pyrrolo[3,4-c]pyrrole-1,4(2H,5H)-dione (EHTPPD-MT), 2Br-EHTPPD (250 mg), TMTD (180 mg) and K_2CO_3 (110 mg) were dissolved in a mixture solvent of tetrahydrofuran (THF, 5 ml) and deionized water (2 ml) by stirring for 20 min. Then tetrakis(triphenylphosphine)palladium(0) ($Pd(PPh_3)_4$, 28 mg) was added to the mixture solution, followed by heating up to 85 ^oC and keeping at this temperature for 16 h in order to proceed the coupling reaction between 2Br-EHTPPD and TMTD. After terminating the coupling reaction by cooling the reaction solution, methanol (Aldrich, 99.8 %) was added to the solution in order to make precipitates. The unreacted starting materials were washed out and then the final precipitates were subject to centrifugation and filtration processes. Next, additional purification processes (column chromatography etc) were carried out before drying in a vacuum oven for 24 h. The colour of the finally dried EHTPPD-MT powder was dark pale blue (yield = 78 %). The mass of the synthesized EHTPPD-MT material was measured with a matrix-assisted laser desorption ionization-time of flight-mass spectroscopy (MALDI-TOF-MS, Voyager DE-STR, Applied Biosystems): *Mass* (*m/z*) = 717.08 (calculated for $C_{54}H_{58}N_4O_6S_2$); 716.33 (measured). Further characterization of the EHTPPD-MT material was carried out with nuclear magnetic spectroscopy (NMR, INOVA 14.1t, Varian unity): ^{13}C-NMR (500 MHz, CDCl3, δ (ppm)) = 165.1(C1, C=O), 14.1 (C18), 23.0 (C17), 29.3 (C16), 32.1 (C15), 37.9 (C14), 47.0 (C13), 11.6 (C19), 26.1 (C20), 121.7 (C11), 125.5 (C9), 15.4 (C12), 137.6 (C10), 137.4 (C8), 138.1 (C7), 136.3 (C4), 127.9 (C5), 132.5 (C6), 142.6 (C3), 113.6 (C2) (see the position of C1~C20 in Fig. S6). To prepare solutions for the BHJ layers, EHTPPD-MT and $PC_{61}BM$ (Nano-C) were dissolved in chlorobenzene at a solid concentration of 40 mg/ml by varying the ratio of EHTPPD-MT to $PC_{61}BM$ (EHTPPD-MT: $PC_{61}BM$ = 1:2 and 1:3 by weight). The binary solutions were subject to vigorous stirring at room temperature for well mixing. The pristine EHTPPD-MT solution was also prepared using the same solvent for comparison.

***Film and Device Fabrication*:** To fabricate devices, indium-tin oxide (ITO)-coated glass substrates (sheet resistance = 10 Ω/□) were patterned to make suitable ITO electrodes by employing a photolithography/etching process, followed by wet (acetone and isopropyl alcohol) and dry (UV-ozone) cleaning steps. The ITO-coated poly(ethylene terephthalate) (PET) as a flexible substrate was patterned for the similar ITO electrodes by using hydrogen fluoride (HF) as an etchant and cleaned with the same cleaning process as for the ITO-glass substrates. Poly(3,4-ethylenedioxythiophene):poly(styrenesulfonate) (PEDOT:PSS) (PH500, HC Starck) solution was spun on the cleaned ITO-glass substrates (and ITO-PET substrates) in order to form a hole-collecting buffer layer (HCBL). The PEDOT:PSS layer (thickness = 45 nm) was annealed at 230 ^oC for 15 min. After cooling the PEDOT:PSS-coated ITO-glass substrates to room temperature, the BHJ layers (thickness = 120 nm) were spin-coated on the PEDOT:PSS layers at 1000 rpm using the binary solutions of EHTPPD-MT and $PC_{61}BM$, followed by soft-baking at 50 ^oC for 30 min. The active layer-coated samples were loaded into a vacuum chamber inside an argon-filled glove box for the deposition of metal electrodes. Aluminium (Al, ~95 nm) top electrodes were deposited by thermal evaporation at a base pressure of $\sim 1\times10^{-6}$ Torr, which led to an exact active area of 0.09 cm^2. All devices fabricated were stored inside the same glove box before measurement. The EHTPPD-MT:$PC_{61}BM$ films were also coated on quartz substrates for the measurements of optical absorption spectra and photoelectron (PE) yield spectra, while they were coated on the PEDOT:PSS layer that was coated on the ITO-glass substrates for the SEM and GIXD measurements.

***Measurement*:** The optical absorption spectra of solutions and films were measured using a UV-visible spectrometer (Optizen 2120 UV, Mecasys), while a PE yield spectrometer (AC-2, Hitachi High Tech) was used for the measurement of ionization potential. The current density – voltage (J-V) characteristics of devices were measured using a specialized photodiode measurement system equipped with a monochromator (CM110, Spectral Products), a light source (Tungsten-Halogen lamp, 150 W, ASBN-W, Spectral Products), series of laser diodes (405 nm, 532 nm and 650 nm, Linelife), and an electrometer (Keithley 2400). The incident light intensity (P_{IN}) was controlled with a neutral density filter set (ANG-series, CVI Melles-Griot) and a calibrated silicon photodiode (818-UV, Newport). The nanomorphology of the pristine EHTPPD-MT and BHJ layers was measured using a scanning electron microscope (SEM, PHI700, ULVAC-PHI) and a field-emission transmission electron microscope (FE-TEM, Titan G2 ChemiSTEM Cs Probe). A synchrotron radiation grazing incidence angle X-ray diffraction (GIXD, 3C-SAXS I, Pohang Accelerator Laboratory) was employed to measure the crystal nanostructure of the pristine EHTPPD-MT and BHJ layers: The X-ray wavelength was 0.11352 nm, while the incidence angle was 0.16^o. The detailed analysis of 2D GIXD images is described in the supporting information (Fig. S5).

Acknowledgements

This work was financially supported by Korean Government grants (Basic Research Laboratory Program_2011-0020264, Basic Science Research Program_2009-0093819, NRF_2012K1A3A1A09027883, Pioneer Research Center Program_2012-0001262, NRF_2012R1A1B3000523, NRF_2014H1A2A1016454, MOTIE_10048434).

Notes and references

Electronic Supplementary Information (ESI) available: Optical absorption spectrum of chlorobenzene (solvent), optical absorption spectrum of EHTPPD-MT in chlorobenzene for checking the absorption edge, optical absorption spectrum of the $PC_{61}BM$ film, fast photoresponse of the OPDI with the EHTPPD-MT:$PC_{61}BM$ (1:2) layer under quick on/off modulation of the high intensity green light, analysis of 2D GIXD image for the pristine EHTPPD-MT film, and assignment of carbon atoms in

the EHTPPD-MT molecule for ^{13}C-NMR spectrum analysis. See DOI: 10.1039/b000000x/

1 W. Cheung, P. L. Chiu, R. R. Parajuli, Y. Ma, S. R. Ali and H. He, *J. Mater. Chem*., 2009, **19**, 6465.
2 X. Liu, Y. –Z. Long, L. Liao, X. Duan and Z. Fan, *ACS Nano*, 2012, **6**, 1888.
3 Y. Kim and C.-S. Ha, *Advances in* Organic *Light-Emitting Devices,* Trans Tech Publications, Switzerland, 2008.
4 E. Saracco, B. Bouthinon, J. –M. Verilhac, C. Celle, N. Chevalier, D. Mariolle, O. Dhez and J. –P. Simonato, *Adv. Mater.*, 2013, **25**, 6534.
5 P. Peumans, A. Yakimov and S. R. Forrest, *J. Appl. Phys*., 2013, **93**, 3693.
6 P. Sonar, G. –M. Ng, T. T. Lin, A. Dodabalapur and Z. –K. Chen, *J. Mater. Chem*., 2010, **20**, 3626.
7 I. Meager, R. S. Ashraf, S. Rossbauer, H. Bronstein, J. E. Donaghey, J. Marshall, B. C. Schroeder, M. Heeney, T. D. Anthopoulos and I. McCulloch, *Macromolecules*, 2013, **46**, 5961.
8 P. Dutta, H. Park, M. Oh, S. Bagde, I. N. Kang and S. –H. Lee, *J. Polym. Sci., Part A: Polym. Chem.*, 2013, **51**, 2948.
9 J. Huang, C. Zhan, X. Zhang, Y. Zhao, Z. Lu, H. Jia, B. Jiang, J. Ye, S. Zhang, A. Tang, Y. Liu, Q. Pei and J. Yao, *ACS Appl. Mater. Interfaces*, 2013, **5**, 2033.
10 B. Walker, A. B. Tamayo, X. –D. Dang, P. Zalar, J. H. Seo, A. Garcia, M. Tantiwiwat and T. –Q. Nguyen, *Adv. Funct. Mater*., 2009, **19**, 3063.
11 A. S. Martin, C. R. Lawrence and J. R. Sambles, *Adv. Mater. Opt. Electron.*, 1997, **7**, 45.
12 D. Braun and A. J. Heeger, *Appl. Phys. Lett.*, 1991, **58**, 1982.
13 J. –I. Anzai, H. Sasaki, A. Ueno and T. Osa, *Macromol. Chem. Rapid Commun.,* 1986*,* **7***,* 133.
14 S. Nam, J. Kim, H. Lee, H. Kim, C. -S. Ha and Y. Kim, *ACS Appl. Mater. Interfaces*, 2012, **4**, 1281.
15 X. Liu, L. Tavares, A. Osadnik, J. L. Lausen, J. Kongsted, A. Lützen, H. –G. Rubahn and J. K. -Hansen, *Org. Electron.*, 2014, **15***,* 1273.
16 M. E. Gemayel, M. Treier, C. Musumeci, C. Li, K. Müllen and P. Samorì, *J. Am. Chem. Soc.*, 2012, **134**, 2429.
17 I. H. Campbell and B. K. Crone, *Appl. Phys. Lett.,* 2009, **95**, 263302.
18 H. Tanaka, T. Yasuda, K. Fujita and T. Tsutsui, *Adv. Mater.*, 2006, **18**, 2230.
19 O. Hofmann, P. Miller, P. Sullivan, T. S. Jones, J. C. deMello, D. D.C. Bradley and A. J. deMello, *Sens. Actuat. B-Chem.*, 2005, **106**, 878.
20 N. A. Stathopoulos, L. C. Palilis, M. Vasilopoulou, A. Botsialas, P. Falaras and P. Argitis, *Phys. Stat. Sol. (a)*, 2008, **205**, 2522.
21 T. Hamasaki, T. Morimune, H. Kajii, S. Minakata, R. Tsuruoka, T. Nagamachi and Y. Ohmori, *Thin Solid Films*, 2009, **518**, 548.
22 J. Jeong, S. Nam, H. Kim and Y. Kim, *IEEE J. Sel. Top. Quantum Electron*, DOI 10.1109/JSTQE.2014.2354649.
23 B. Luszczynska, M. Z. Szymanski, J. M. Verilhac, P. Reiss and D. Djurado, *Org. Electron*., 2013, **14**, 3206.
24 J. D. Zimmerman, V. V. Diev, K. Hanson, R. R. Lunt, E. K. Yu, M. E. Thompson and S. R. Forrest, *Adv. Mater.*, 2010, **22**, 2780.
25 N. S. Sariciftci, L. Smilowitz, A. J. Heeger and F. Wudl, *Science*, 1992, **258**, 1474.
26 J. –T. Chen and C. –S. Hsu, *Polym. Chem.*, 2011, **2**, 2707.
27 Y. –J. Cheng, S. –H. Yang and C. –S. Hsu, *Chem. Rev*., 2009, **109**, 5868.
28 H. Kim, S. Nam, J. Jeong, S. Lee, J. Seo, H. Han and Y. Kim, *Kor. J. Chem. Eng*., 2014, **31**, 1095.
29 N. M. M. Pires and T. Dong, *Sensors*, 2013, **13**, 15898.
30 P. E. Keivanidis, F. Laquai, I. A. Howard and R. H. Friend, *Adv. Funct. Mater.*, 2011, **21**, 1355.
31 S. Valouch, C. Hönes, S. W. Kettlitz, N. Christ, H. Do, M. F.G. Klein, H. Kalt, A. Colsmann and U. Lemmer, *Org. Electron.*, 2012, **13**, 2727.
32 S. Gélinas, A. Rao, A. Kumar, S. L. Smith, A. W. Chin, J. Clark, T. S. van der Poll, G. C. Bazan and R. H. Friend, *Science*, 2014, **343**, 512.
33 L. Beverina, R. Ruffo, M. M. Salamone, E. Ronchi, M. Binda, D. Natali and M. Sampietro, *J. Mater. Chem.*, 2012, **22**, 6704.
34 L. Li, Y. Huang, J. Peng, Y. Cao and X. Peng, *J. Mater. Chem. C*, 2014, **2**, 1372.
35 J. Qi, L. Ni, D. Yang, X. Zhou, W. Qiao, M. Li, D. Ma and Z. Y. Wang, *J. Mater. Chem. C*, 2014, **2**, 2431.
36 A. K. Pandey, K. D. Johnstone, P. L. Burn and I. D. W. Samuel, *Sens. Actuat. B*, 2014, **196**, 245.
37 M. Turbiez, R. A. J. Janssen, M. M. Wienk, H. J. Kirner, M. Dueggeli, B. Tieke and Y. Zhu, *World Patent WO2008000664*, 2008.
38 G. Yu, J. Gao, J. C. Hummelen, F. Wudl and A. J. Heeger, *Science*, 1995, **270**, 1789.
39 X. Yang and A. Uddin, *Renew. Sust. Energ. Rev.*, 2014, **30**, 324.
40 Y. Kim, J. Nelson, T. Zhang, S. Cook, J. R. Durrant, H. Kim, J. Park, M. Shin, S. Nam, M. Heeney, I. McCulloch, C.-S. Ha and D. D. C. Bradley, *ACS Nano*, 2009, **3**, 2557.
41 M. T. Dang, L. Hirsch, G. Wantz, and J. D. Wuest, *Chem. Rev.*, 2013, **113**, 3734.
42 M. Shin, H. Kim and Y. Kim, *Macromol. Res*., 2010, **18**, 709.
43 S. Nam, S. Lee, I. Lee, M. Shin, H. Kim and Y. Kim, *Nanoscale*, 2011, **3**, 4261.
44 C. Y. Bing, A. A. Mohanan, T. Saha, R. N. Ramanan, R. Parthiban and N. Ramakrishnan, *Microelectron. Eng.* 2014, **122**, 9.
45 P. Wangyang, Y. Gan, Q. Wang and X. Jiang, *J. Mater. Chem. C*, 2014, **2**, 6140.
46 G. Patern`o, A. J. Warren, J. Spencer, G. Evans, V. G. Sakai, J. Blumbergera and F. Cacialli, *J. Mater. Chem. C*, 2013*,* **1***,* 5619.

[Table of Contents Entry]

Organic photodetectors with solution-processed all-small-molecular bulk heterojunction layers detect near UV light and stable under high-intensity-lights stronger than sun light